JOURNAL OF CATALYSIS 73, 104–119 (1982)

UHV Studies of the Interaction of CO with Small Supported Metal Particles, Pd/Mica

D. L. DOERING, H. POPPA,[1] AND J. T. DICKINSON[2]

Stanford/NASA-Ames Joint Institute for Surface and Microstructure Research, NASA, Ames Research Center, Moffett Field, California 94035

Received May 5, 1981; revised September 21, 1981

The interaction of carbon monoxide with small palladium particles supported on UHV-cleaved and heat-treated single-crystal mica was studied. The Pd particles were characterized and tested using the techniques of flash thermal desorption, Auger electron spectroscopy, core electron energy loss spectroscopy, and transmission electron microscopy. Evidence is presented for CO decomposition on Pd particles during CO adsorption–desorpition experiments. The rate of CO decomposition increased rapidly with diminishing particle size. Residual carbon from CO decomposition blocked CO adsorption and had a strong poisoning effect on the CO oxidation reaction.

INTRODUCTION

Transition metals are frequently used in heterogeneous catalytic reactions. To understand the fundamentals of such reactions, a great deal of research has been devoted to the surface structure and gas–metal interactions of clean, well-characterized single and polycrystalline bulk metal surfaces under ultrahigh-vacuum (UHV) conditions. Similar studies under well-defined conditions have recently begun on supported particulate metal films (*1–4*). These model studies are conducted in the hope of isolating behavior unique to small particles which could be important to catalytic processes.

Average particle size is frequently considered to be one of the more significant parameters affecting the catalytic properties of metal clusters. Attributes that may vary with cluster size include particle shape, defect density, electronic band structure, and possibly crystallography, all of which might affect catalytic behavior. For supported particles, the metal–substrate interaction must also be considered. In terms of gas–metal interactions, changes in binding energy, adsorption stoichiometry, and/or reaction kinetics can be affected by cluster-size-dependent metal properties.

The interaction of CO and oxygen with single-crystal Pd surfaces of varying orientation has been well studied. No CO decomposition has been found on these surfaces (in the absence of an electron beam) (*5–8*). However, in a recent report (*3*), we presented evidence for CO decomposition on small Pd particles supported on mica; this suggested that important differences between large-area bulk single crystals and small supported particles existed. Since CO decomposition on Pd had not been observed in the past, our results were unexpected and additional experimental evidence was desirable.

This report presents results of a more detailed study of CO interaction with small supported Pd particles of varying size; it also addresses the questions of how residual carbon from decomposed CO affects the activity of the metal surfaces and how the reaction with oxygen alone to form CO_2 can be used as chemical evidence for the existence of surface C.

[1] To whom correspondence should be addressed.

[2] Permanent address: Physics Department, Washington State University, Pullman, Wash. 99164.

0021-9517/82/010104-16$02.00/0

EXPERIMENTAL

Particulate Pd films were grown on UHV-cleaved and heat-treated mica at a substrate temperature of 200°C and with a metal flux of 1.6×10^{14} atoms/cm^2/sec (about 1.4 nm/min) for all samples. Deposition times usually ranged from 1 to 50 sec. During deposition the background pressure was usually about 3×10^{-9} Torr (1 Torr = 133.3 Nm^{-2}). Details of the preparation and testing procedures were presented in the preceding paper (*4*).

Pd particles supported on mica were characterized using flash thermal desorption (FTD), Auger electron spectroscopy (AES), and core electron energy loss spectroscopy (CEELS). Flash thermal reaction spectroscopy (FTRS) is introduced to determine the effect of surface carbon on the CO oxidation reaction. Particles were further characterized by transmission electron microscopy (TEM).

We previously employed a cylindrical mirror analyzer (CMA) with a fixed integral electron gun (*3, 4*) which was replaced during this study with a CMA with a scanned electron gun. Scanning the electron beam had two main advantages. First, it allowed the use of a higher primary electron beam current (10 μA), while maintaining a low current density. This resulted in a higher total Auger signal strength, but limited any decomposition of the mica and the interaction of any adsorbed CO with the probing electron beam (*9, 10*). Second, by sweeping the electron beam and detecting the secondary electron signal, a low-magnification SEM image of the sample could be displayed on a video monitor. Thus, the sample could be accurately positioned for AES and CEELS analyses.

CO and/or oxygen was introduced into the system, to pressures usually less than 1×10^{-7} Torr (total pressure), for adsorption or reaction tests. Higher pressures were only used during gas–thermal treatments to determine their effects on the shapes and dispersions of the Pd particles. Specific treatment conditions will be discussed where applicable.

Because samples are exposed to atmosphere during the preparation and transfer process for TEM, concern exists as to whether the state of the sample observed by TEM is representative of the state prior to removal from the UHV chamber. To address this concern, experiments have begun where metal particles are grown *in situ* in the TEM followed by exposure to atmosphere. Initial studies by Anton (unpublished data) of small Pd particles (as small as 1 nm) grown on recrystallized alumina have shown no observable change in the deposit after air exposure. Therefore, the micrographs of samples used in this work are assumed to be representative of the "pre-air exposure" state. Studies of the interaction of other metals with the atmosphere are in progress.

RESULTS

1. Sample Characterization

Each of a set of samples prepared with various Pd exposures was analyzed by AES, tested with various gas exposures, and cleaved from the parent mica block. Then the set was removed from the system to be examined by TEM. For Pd-deposition times less than 50 sec, the average particle size distribution was relatively narrow (width about half of the average particle size). Examples of the Pd deposits are shown in Fig. 1. The mean particle diameter increases uniformly with deposition time from 1.9 nm (1-sec Pd deposit) to 7.6 nm (50-sec Pd deposit) as shown in Fig. 2. However, accurate identification and sizing of Pd particles on mica smaller than 2.0 nm was very difficult. Therefore, the average sizes of samples with short deposition times may be slightly overestimated. The particle number density was between 6 and 8×10^{11} cm^{-2} up to a 25-sec deposit. Further deposition resulted in massive coalescence which reduced the number density.

Transmission electron diffraction pat-

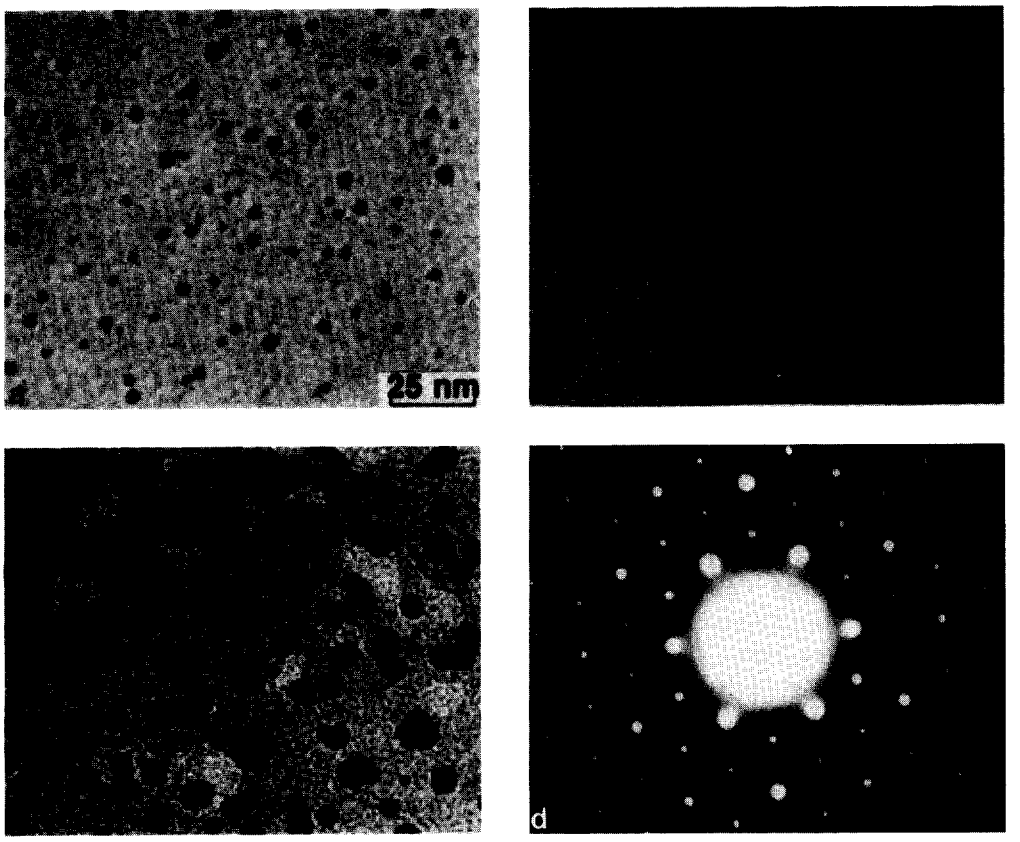

FIG. 1. Representative transmission electron micrographs of particulate Pd films on mica: (a) 2-sec metal deposition time (2.7 nm average size), (b) 15-sec deposition time (42 nm), (c) 50-sec deposition time (7.6 nm), (d) transmission electron diffraction pattern of the deposit in (b). The metal flux and substrate temperature during deposition were 1.4 nm/min and 200°C, respectively.

terns of the specimens showed some texture indicating the tendency for epitaxial growth of Pd on mica (see Fig. 1d). Since the (220) Pd ring was the most intense, the particles must have a preferred orientation of their (111) planes parallel to the substrate. The degree of epitaxial ordering increased with deposition time. Better epitaxy could also be produced when higher substrate temperatures were used (*1, 11*), but only samples grown at a 200°C substrate temperature will be considered here.

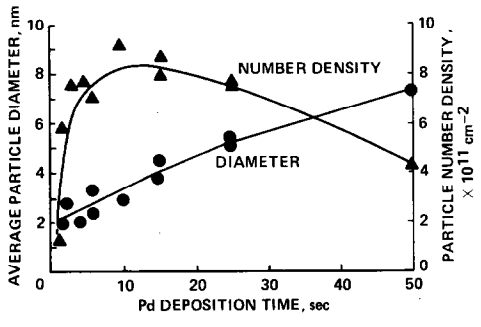

FIG. 2. Average diameter and number density of Pd particles grown on mica vs deposition time. The Pd flux and substrate temperature during deposition were 1.4 nm/min and 200°C, respectively.

Auger analysis was performed on all samples immediately after deposition (after sufficient cooling from deposition temperature) and was followed by a thermal desorption of CO from a saturation CO dose (except for a sample set removed without desorptions for TEM study of the "as-deposited" state). For low metal coverages, the peak–peak height of the 330-eV Pd Au-

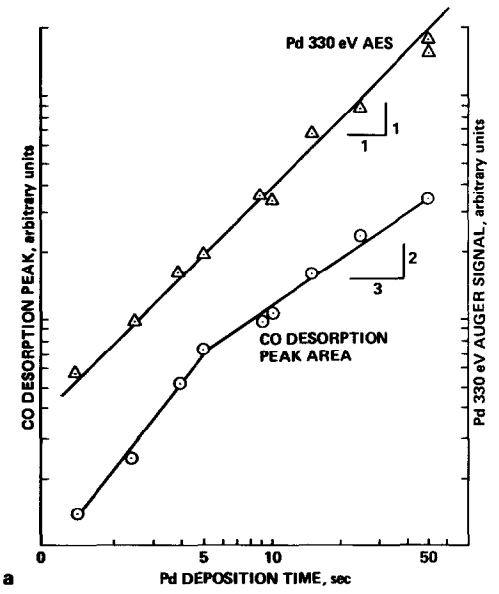

FIG. 3a. The peak-to-peak height of the 330-eV Pd Auger signal and the area under the CO desorption peak vs Pd deposition time plotted on a log–log scale.

ger signal measured the relative amounts of metal deposited on the surface. The area under a CO desorption peak is proportional to the total amount of CO desorbed from the sample because of the high pumping speed of the cryopump (*12*). For a saturation dose and assuming all samples have a constant adsorption stoichiometry, this desorption peak area is thus a relative measure of the surface area of different samples.

The Pd Auger signal and the CO desorption peak area are plotted in Fig. 3a as a function of metal deposition time. On a log–log scale, both curves were linear for very small particles. During the very early stage of deposition this is expected because particles are small and almost all of the metal atoms are on the particle surface (dispersion = 1.0). As the particles become larger (over 5 sec deposition time), atoms in the interior of the cluster no longer contribute to the CO desorption signal and the desorption peak area vs deposition time tends toward a slope of two-thirds. If the metal volume increases linearly with deposition time, which is consistent with the linearly increasing Pd Auger signal, a slope of two-thirds would yield the expected surface-to-volume relationship for particles growing three dimensionally. Of course, for deposition times longer than the range used here, coalescence of the particles would further influence this slope. Over about 20 sec of deposit, attenuation of the Auger signal from "bulk" atoms begins to affect the Auger signal (the escape depth of the 330-eV Pd Auger electrons is about 0.8 nm (*13*)) and the deviation from linear behavior begins.

An important comparison was also made between the metal surface area as measured by CO desorption and that determined from the TEM. The "TEM" metal surface area was obtained by assuming that the particles were hemispherical. The average particle area was found from the size distribution and then multiplied by the number density to give the total metal surface area per square centimeter of sub-

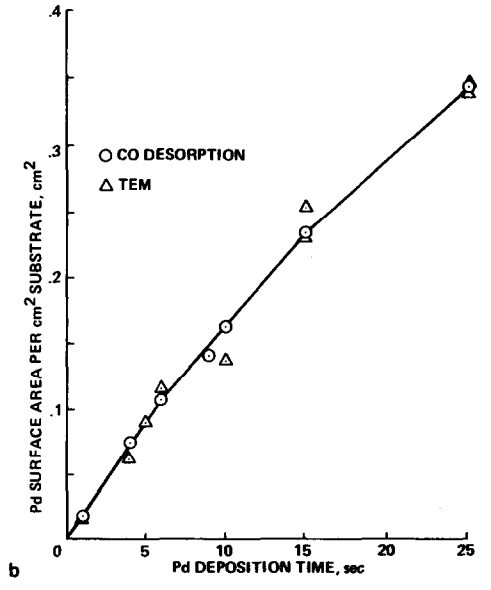

FIG. 3b. Comparison of the Pd surface area as measured by the CO desorption peak area and calculated from TEM micrographs. The two areas were normalized to be equal for the 25-sec deposit.

strate. The two methods of area measurement were normalized such that the values for a 25-sec deposit were equal; for a continuous metal film, the CO desorption based on this normalization yields an area of about 1.0 cm^2, as expected. Figure 3b shows clearly that the agreement of the TEM and CO desorption areas for short deposition times is very good, thus indicating that most of the metal surface measured by FTD is accounted for in the TEM micrographs. Therefore, the possibility of large proportions of deposited Pd existing in such a high state of dispersion that detection by TEM is impossible is excluded. As a consequence, all chemical effects that will be described later in this report are attributed to TEM-detected Pd particles. By comparing the calculated metal volume from TEM micrographs with the volume of the metal exposure as measured by a quartz crystal microbalance, a reasonable sticking coefficient of 0.6 is found (*14*).

The first CO desorptions from samples with different metal exposures are shown in Fig. 4. Each desorption spectrum was taken 15 min after Pd deposition to allow samples to cool to an adsorption temperature of about 50°C. The temperature of the main desorption peak for these spectra (as inferred from temperature calibrations) was 160°C for all deposits. Assuming a constant preexponential factor of 1×10^{13} sec, a CO activation energy of desorption of about 27 kcal/mole can be calculated for comparison with other CO on Pd work. Previously, it was shown that CO desorption from Pd particles was first order and could be described by a coverage-dependent activation energy (*1*). When normalized to the same peak height, the shapes of these desorption peaks were observed to be nearly constant, which implies that the desorption behavior is followed over the entire range of particle sizes studied. (The high-temperature contribution for the CO desorption from a 50-sec deposit is found only for large particles and is assumed to be associated with steps on the Pd induced by coalescence, because

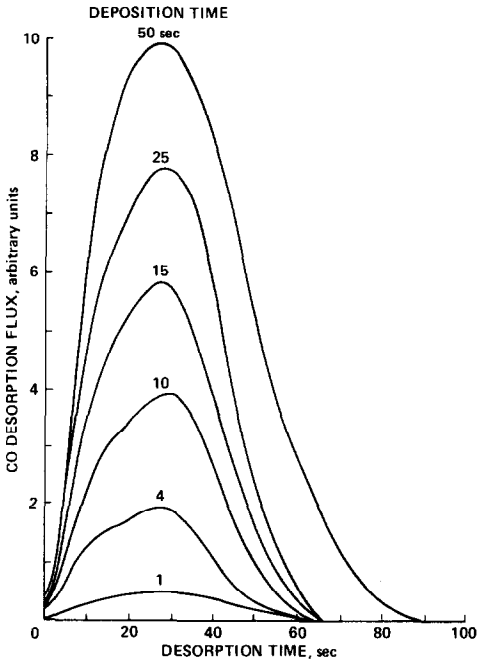

FIG. 4. First CO desorptions from particulate Pd films with various metal exposures. (The metal flux and substrate temperature during deposition were 1.4 nm/min and 200°C, respectively.) The CO dose for all samples was 6 L (6×10^{-6} Torr sec).

similar desorption features were found for CO on stepped Pt (111) by Collins and Spicer (*15*).) The shoulder on the low-temperature side of the peak was also observed by Ladas *et al.* from small Pd particles supported on sapphire (*16*). There, the lower binding state was dominant for 1.5-nm-diameter particles.

2. *CO-Induced Contamination of Pd Particles*

Successive CO adsorption–desorption cycles from a saturation dose produced a continuous reduction of the CO desorption peak area from small Pd particles. This was in contrast to results for bulk single crystals of Pd, where no evidence was found for CO-induced contamination (*6*). (The buildup of C by electron beam exposure of CO-covered bulk Pd (*10*) is, of course, a different phenomenon.) Initially, the decay of the CO desorption peak is proportional

to the number of desorptions, but the reduction of the peak area slows appreciably for large reductions of the CO desorption peak area. Although coalescence and sintering are thought to occur (*3*), neither AES nor TEM shows enough change to account for all of this loss. Therefore, contamination of the Pd surface is the only alternative. Since heating of the Pd/mica sample in the residual background pressure ($<5 \times 10^{-10}$ Torr) does not induce the reduction of the CO peak, contamination from the mica of background gases is very unlikely. Therefore, the contamination must be CO induced.

Figure 5 shows CO desorption spectra from successive 6-L CO doses (at a 50°C adsorption temperature) for a Pd deposit of 2.3 nm in average particle diameter. (Note: 1 L = 10^{-6} Torr sec.) The average reduction of the desorption peak area per flash will be referred to as the CO desorption decay rate. In the case of Fig. 5, the decay rate is about 10%. The desorption peak maximum

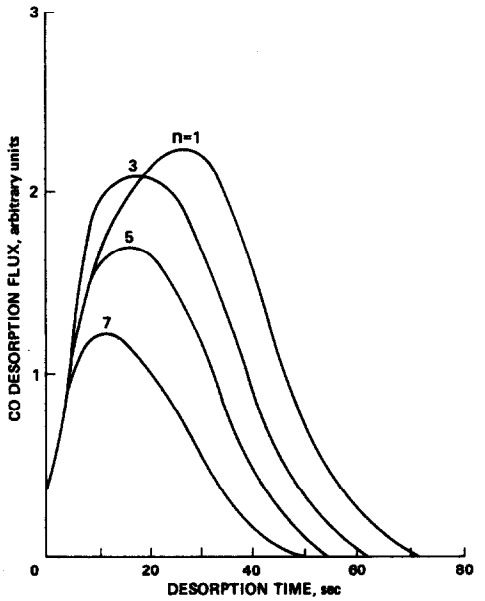

FIG. 5. Successive CO desorptions from Pd particles from a 5-sec deposit at the standard metal flux and substrate temperature during deposition (average particle diameter of about 2.3 nm). *n* is the desorption number in series.

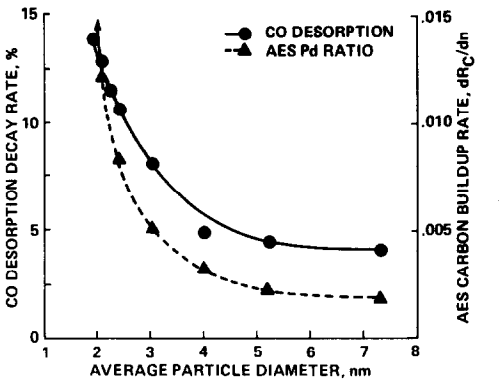

FIG. 6. Comparison of the CO desorption decay rate and the rate of carbon buildup as measured by AES for varying average particle diameter.

also shifted to lower temperatures due to two different mechanisms. The shift in the peak position between the first and third desorptions shown in Fig. 5 can be induced by thermal treatments alone, as reported previously (*3*), and is attributed to refaceting of the particle surfaces upon heating. The peak shift observed for $n = 3$ to $n = 7$ in Fig. 5 was much more gradual and caused by the preferred elimination of the high-temperature portion of the peak. This suggests that the contaminant preferably blocks the higher-energy CO adsorption sites (*3*).

The CO desorption decay rate as a function of particle size was also studied in detail because, as in the case of small Ni particles (*4*), the decay rate seemed to increase rapidly with diminishing particle size. For larger particles and upwards to continuous Pd films, the desorption decay rate was negligible, which agrees with results found for bulk single crystals (*2*, *6*). The high decay rates for small Pd particles, as shown in one of the curves in Fig. 6, indicate that the particle contamination reaction is strongly size dependent for supported Pd particles on mica.

Contamination of the particles could also be produced by steady-state heating of the Pd/mica sample in CO. As seen in Fig. 7 for a 25-sec Pd deposit, where the CO peak decay of a series of consecutive desorp-

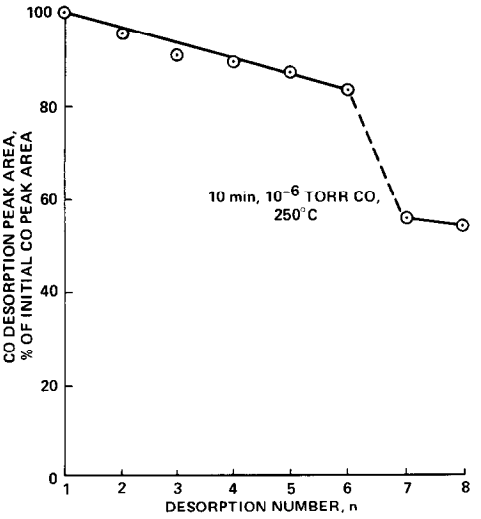

FIG. 7. The area of the CO desorption peak from a 25-sec Pd deposit during successive desorptions and after an extended heat treatment in CO (10 min at 250°C in 10^{-6} Torr CO).

tions is compared with the decay caused by a 10-min exposure to 10^{-6} Torr CO at 250°C, a much stronger decay of the corresponding CO desorption peak can be obtained. From these results, the probability for CO decomposition under these reaction conditions can be calculated to be between 10^{-3} and 10^{-4}. This is comparable to the CO decomposition rate estimated for RH (111) (*17*). During successive temperature-programmed CO adsorption–desorption cycles, the CO decomposition probability must be much higher, however. The reason for this difference is not yet clear.

3. Detection of Carbon on Palladium

Carbon decomposed from CO is the most likely candidate for the CO-induced contamination buildup observed in this work. However, direct detection of carbon on Pd by AES was not possible due to the overlap of the C 272-eV and the Pd 279-eV Auger peaks. Carbon can, however, be indirectly measured by monitoring changes in the ratio (R_c) of the principal Pd peaks (279 eV/330 eV). Carbon accumulation on the Pd would cause an increase of the combined peak (279 eV) and a slight decrease in the 330-eV Pd main Auger peak. Thus R_c increases with C buildup, its change being proportional to the amount of C to first order. For a large amount of C, the influence of carbon shifts the combined peak toward a lower energy. For small Pd particles, this increase of R_c always accompanied the CO desorption peak decay.

The average change per desorption in the Pd Auger peak ratio (dR_c/dn) as a function of particle size is displayed in Fig. 6 along with the CO desorption peak decay rate. It is obvious that the two curves share essentially the same trend. This similarity further substantiates the contention that carbon is the surface contaminant in question.

Another method of carbon detection on Pd by AES is to subtract the spectrum of a clean Pd sample from that of a contaminated one. For this purpose, the analog Auger spectra were digitized by hand over the energy range from 250 to 300 eV. The digital data were then processed by a Hewlett–Packard 9830 calculator. The signals were normalized to the clean 330-eV Pd peak height to account for attenuation of that peak with increasing carbon coverage. The difference spectrum, then, reveals the carbon Auger peak. Figure 8 shows the resulting carbon difference spectrum as a function of increasing contamination of a 15-sec Pd deposit. Contamination was produced by a series of CO flash thermal desorptions. (This specific sample was chosen because it had previously been shown to contaminate quickly due to a high heating rate during CO desorption and the corresponding R_c changed dramatically with successive desorptions (*3*)). The Auger difference peak in Fig. 8, although noisy due to digitizing by hand, occurs at 273 eV which is expected for C. After a heat treatment in oxygen (15 min at 5×10^{-7} Torr at 300°C), the carbon signal almost vanishes (last spectrum in Fig. 8). Thus, this technique successfully displayed the C Auger peak on Pd directly in this case. However, it was found that the monitoring of R_c is simpler, more sensitive

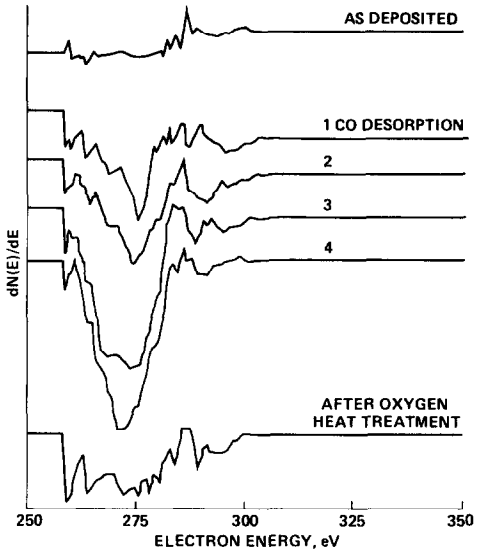

FIG. 8. Digitally processed Auger difference spectra ranging from 250 to 300 eV for a 15-sec deposit subjected to successive CO desorptions at a high heating rate.

to small amounts of carbon on Pd, and therefore more useful for evaluating large numbers of spectra. However, digital acquisition and processing of Auger signals could make this type of spectrum subtraction an experimentally useful method of detecting carbon on Pd.

Because of the controversial nature of the CO–Pd interaction leading to the existence of C on Pd particles, it was important to provide another spectroscopic proof for C by using core electron energy loss spectroscopy (CEELS) (M. Prutton, private communication). Although the Auger peaks of Pd and carbon overlap, the core ionization levels are well separated in energy (*18*). Therefore, C should be unambiguously identified in the electron energy loss spectrum as well. Figure 9 displays the Pd, K, and C loss peaks in a hand-digitized and computer-smoothed loss spectrum of a highly C contaminated Pd/mica sample. The Pd, K, and C peaks are easily separated in spite of a rather low signal-to-noise ratio and a sharply sloping background level (indicated by the broken line in Fig. 9). The loss spectrum was acquired with the CMA in differentiated form using a relatively high primary beam current of 10 μA in order to increase the signal level of the loss peaks which were about 100 times smaller than the respective Auger peaks; the primary electron beam was scanned over the CMA acceptance area of the sample to minimize beam effects on the mica (*9*). The primary beam energy of 700 eV maximized the loss signals in this case.

Because the carbon loss signal is so small compared to the adjacent K peak from mica, CEELS required relatively large amounts of C for more systematic studies. Successive heat treatments of a 25-sec Pd deposit in CO (15 min at 300°C in 10^{-6} Torr) caused large increases of carbon on the sample. Before and after each treatment, a standard CO desorption spectrum from a saturated dose and a CEELS spectrum were recorded. The corresponding results are summarized in Fig. 10. No carbon was found for a freshly prepared sample. The CO desorption peak area was strongly reduced, as expected, with each heat treatment (see Fig. 10a) and a corresponding carbon peak appears in the loss spectrum

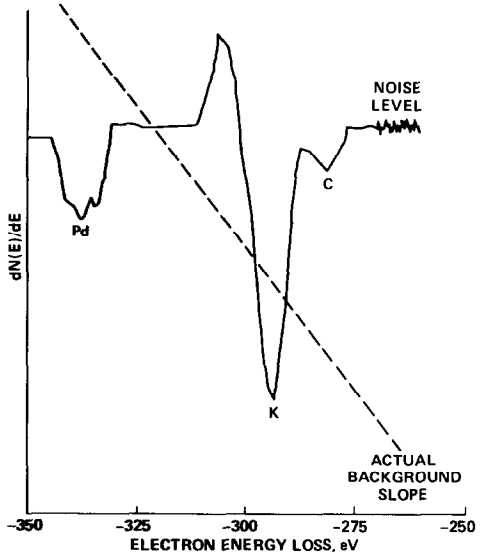

FIG. 9. The differential energy loss spectrum of partially carbon covered Pd particles on mica over the energy range from −350 to −260 eV.

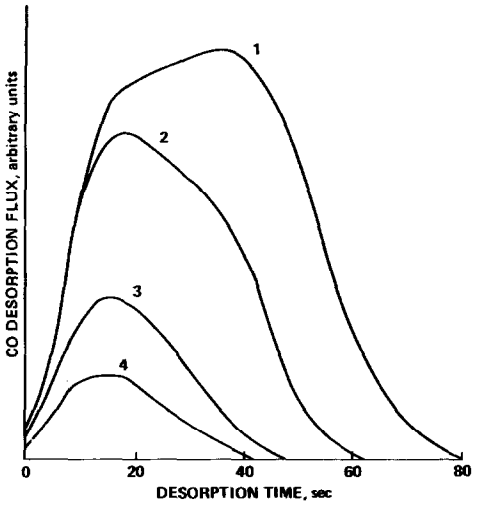

FIG. 10a. C buildup on a Pd deposit by successive heat treatments in CO (15 min at 300°C in 10^{-6} Torr CO). Detection by CO thermal desorptions before (1) and after each treatment (2–4).

(see Fig. 10b). Assuming the same relative peak positions of the C and K losses as in XPS (X-ray photoelectron spectroscopy) (*18*), the carbon-loss peak position is similar to that of a metal carbide. However, when most of the surface is contaminated the C-loss peak seems to move closer to the K peak. This lower loss energy may be indicative of a more "graphite-like" carbon phase with C–C bonds (see Fig. 10b, curve 4).

To add chemical proof to the electron spectroscopic evidence for carbon on the Pd particles, contaminated Pd/mica samples were flash heated in an oxygen background. This technique, referred to as flash thermal reaction spectroscopy (FTRS), was easily adapted to the existing experimental system producing CO_2 reaction peaks as a function of time after insertion of the sample into an oven. This is similar to the well-established method of temperature-programmed surface reaction (TPSR) (*19*), the only difference being the temperature profile necessitated by our experimental approach. Figure 11 shows FTRS spectra of a 15-sec Pd deposit with varying degrees of C contamination in a 370°C oven in a system background of 5×10^{-8} Torr of oxygen. The Pd sample was contaminated by either repeated CO desorptions or by electron beam irradiation in a high-pressure CO environment (10^{-7} Torr). (In order to prevent any reaction of the oxygen with CO preadsorbed from the background gas, the sam-

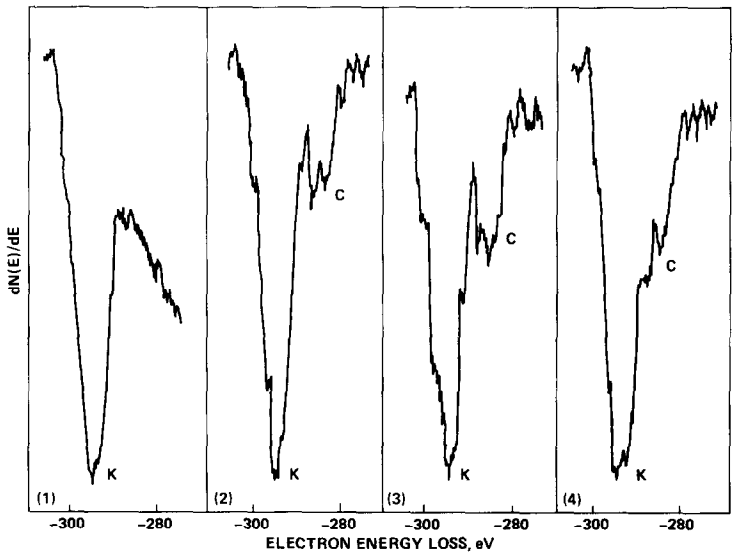

FIG. 10b. Detection by core electron energy loss spectroscopy. (Curve numbers refer to respective heat treatments as in Fig. 10a.)

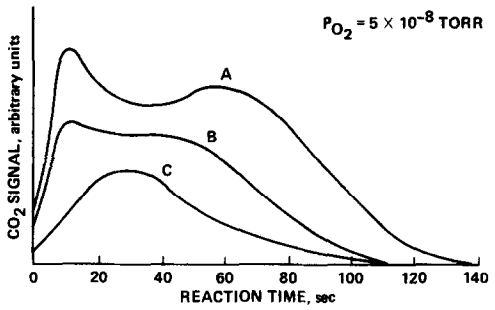

FIG. 11. Flash thermal reaction spectra (FTRS) of CO_2 from differently produced surface C on a 15-sec Pd deposit in an oxygen background of 5×10^{-8} Torr O_2. (A) After six CO desorptions, (B) after the sample was recontaminated by 15 min of exposure to the scanned electron beam in 10^{-7} Torr CO, and (C) after recarburizing the sample by only one CO desorption. No CO_2 is produced during FTRS of either freshly prepared or oxygen-"cleaned" Pd samples.

ple was heated for 60 sec shortly before O_2 was leaked into the system.)

The FTRS results of Fig. 11 are reproducible in general, but detailed CO_2 peak assignments must be left for future studies (small CO peaks are lost due to a substantially increased CO background level caused by the interaction of O_2 with hot ionizer filaments). However, there is no doubt that: (a) clean Pd particles produce no CO_2 signal during FTRS, (b) very small amounts of surface C can be detected easily in this way (see Fig. 11, line C), and (c) surface C produced by electron beam dissociation, steady-state heating in CO, or CO flash desorptions leads to similar CO_2 FTRS spectra. The last point, in particular, further supports the contention that CO decomposes on small Pd particles.

4. *Inhibition of CO Oxidation on Pd by Surface Carbon*

The CO oxidation reaction on small Pd particles supported on sapphire has been studied in detail by Ladas *et al.* (*16*). Their results were consistent with those on large single crystals of Pd and the reaction was found insensitive to the Pd surface structure. In this study of small Pd particles on mica, the vacuum system was not well suited for a detailed study of steady-state reactions. Therefore, aspects of the CO oxidation reaction were examined for small Pd particles on mica by FTRS.

From single-crystal Pd studies, it was known that the CO oxidation reaction follows the Langmuir–Hinshelwood mechanism where both species must be adsorbed to react (*20*), and that a saturated CO layer prevents oxygen adsorption and thus stops CO oxidation. Therefore, adsorption of 3 L of CO preceded each FTRS test.

The effect of preadsorbed CO on the CO oxidation reaction spectrum of a 100-sec Pd deposit was determined by FTRS in a background of 5×10^{-8} Torr O_2. The partial pressures of CO and CO_2 could be monitored simultaneously as a function of time by a quadrupole mass spectrometer (QMS) with a programmable mass peak selector. The results are compared in Fig. 12 with a standard CO desorption (broken curve). Only CO is desorbed from the sample until surface sites are available for oxygen adsorption and dissociation. Then, the CO_2 signal begins to rise to a maximum at about 40 sec after which depletion of CO occurs.

A similar FTRS test was conducted (see Fig. 13) except that both carbon monoxide and oxygen were leaked into the system at equal partial pressures of 5×10^{-8} Torr. As the sample temperature increased upon in-

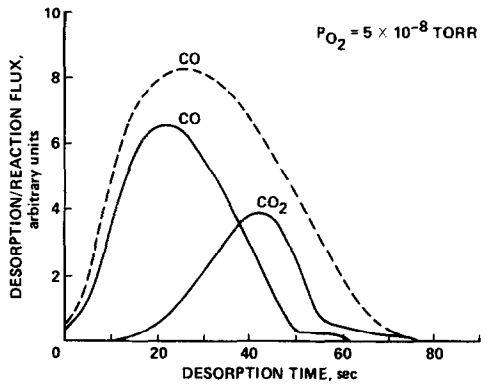

FIG. 12. Flash thermal reaction of CO preadsorbed on Pd particles with a constant O_2 background of 5×10^{-8} Torr. (The broken line indicates a standard CO desorption under UHV, for comparison.)

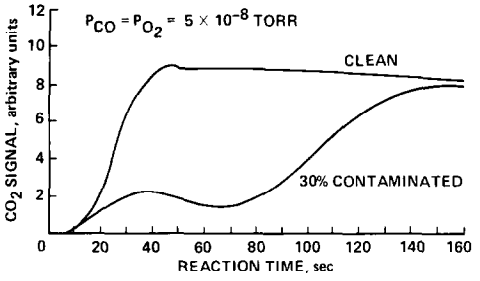

FIG. 13. Flash thermal reaction spectra of clean and carbon-contaminated Pd particles in 5×10^{-8} Torr CO and O_2, respectively. Prior to flashing 3 L of CO is preadsorbed onto the Pd.

sertion of the Pd/mica sample into the oven, CO desorption opened sites for oxygen adsorption and the standard oxidation reaction could begin. The "clean" reaction spectrum of a fresh 50-sec Pd deposit is shown in Fig. 13. After all of the preadsorbed CO is desorbed, an equilibrium level of the CO_2 signal is reached at about 65 sec. The sample temperature above this point continues to increase slowly, but it corresponds roughly to the temperature of the maximum CO oxidation rate found during steady-state studies of single-crystal and small particle specimens (*16*, *20*). The CO_2 production was measured for samples with different Pd deposition times (corresponding to different particle sizes; see Fig. 2). The CO oxidation rate was found independent of particle size which agrees well with the results for small Pd particles on sapphire (*16*).

Pd samples contaminated by carbon (from several CO adsorption–desorption cycles) exhibited a drastic reduction in the CO oxidation rate. As seen for the 50-sec Pd deposit in Fig. 13, the Co_2 peak at 40 sec due to preadsorbed CO is still present, but is significantly reduced from that of a clean sample. The equilibrium CO_2 level reached at about 65 sec (see Fig. 13) is also greatly reduced indicating a significant loss of reactivity. For the sample of Fig. 13, the CO desorption peak area was reduced only 30%, but the CO_2 production level at 65 sec was diminished by nearly 80%. Oxygen has a low packing density on Pd (*21*), needs adjacent sites to dissociate, and may need preferred positioning relative to the adsorbed CO to react. Thus, it is not unreasonable that such a large reduction in CO_2 production occurs for a relatively small loss of the CO desorption peak area. For reaction times longer than about 65 sec (see Fig. 13) (and over temperatures of about 250°C), a second rise in the CO_2 production level occurs until that of a clean sample is nearly achieved. A subsequent CO desorption test of the "cleaned" sample shows a recovery of much of the lost peak area (which is accompanied by the expected reduction of R_c). Thus, it is concluded that the carbon residue is removed from the Pd during the CO oxidation reaction, presumably as CO or CO_2. Removal of C (and S) from Pd during the CO oxidation reaction was also reported by Ertl and Koch (*22*). Effective C removal was always found except for extremely contaminated samples. In this case, no reaction or cleaning is observed, probably because clean Pd sites are not available.

5. *Effect of Gas–Thermal Treatments on Pd Particles*

Dramatic changes in the morphology of Ni particles were reported in the preceding paper (*4*) as the result of heat treatments in background gases such as CO, O_2, or H_2. In a similar manner, five samples each with nominally identical 15-sec Pd deposits were exposed to various gas–thermal treatments and investigated by TEM. All samples had about 8×10^{11} particles/cm^2 and the average particle sizes ranged from 4.0 to 4.3 nm. The treatments included: (1) no treatment or "as deposited," (2) heating in 10^{-6} Torr of CO at 300°C for more than 15 min, (3) heating in 10^{-6} Torr of O_2 at 300°C for 15 min, (4) several CO desorptions and flash heatings in 5×10^{-8} Torr of O_2, and (5) heating in 10^{-6} Torr CO_2 at 300°C for 30 min. TEM micrographs from samples exposed to treatments 1, 2, and 3 are shown in Fig. 14 (for details of TEM specimen prepa-

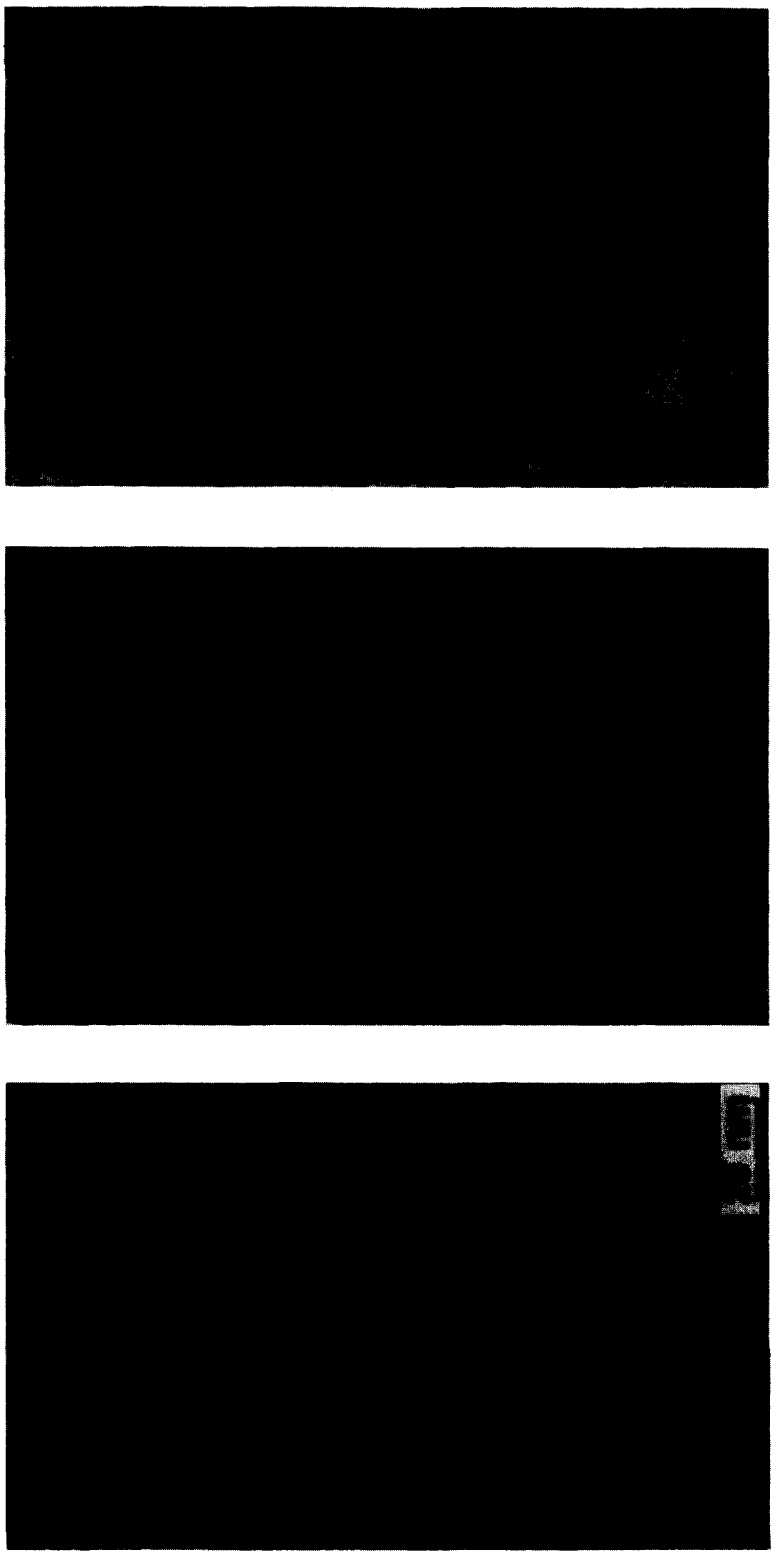

FIG. 14. The effect of gas–thermal treatments on the microstructure of Pd particles (15-sec deposit) supported on mica. TEM results for (a) as deposited, (b) heat treated in CO (30 min, 300°C at 10^{-6} Torr), and (c) heat treated in oxygen (15 min, 300°C at 10^{-6} Torr).

ration see (*23*)). Samples exposed to treatments 4 and 5 are not shown but results were very similar. In contrast to Ni (*4*), no obvious changes of the average particle size or number density were found. (Although subtle differences in particle shape or epitaxy cannot be conclusively ruled out from these preliminary results. Some evidence, for instance, was found for slight improvements of particle shapes by faceting processes.) More detailed *in situ* TEM studies will be necessary to provide reliable results, especially for very small particles.

DISCUSSION

It is known that the adsorption stoichiometry of gases on metals can depend on particle size (*24*). A change of the principal type of binding site with particle size is possible and would be accompanied by a shift in the binding energy. The adsorption stoichiometry can also be affected by substrate interactions. In the case of Pd on mica, normalization of the CO desoprtion peaks presented in Fig. 4 shows no substantial change in the peak shape or position with particle size (to about 2.0 nm diameter; see Figs. 4 and 2). Furthermore, the same Pd surface area was measured by TEM and CO desorption over the entire range of metal deposition (Fig. 3b). These two results suggest that there is no change in the adsorption stoichiometry with particle size. A consequence of this important result is that the total amount of CO desorption flux is a good measure of the relative surface area of particulate Pd deposits on mica. This is especially important since the CO desorption signal is found well above the noise level of the QMS even for particle sizes smaller than 2 nm, and is often very difficult to detect by TEM (*2*).

The CO desorption peak is, therefore, a very sensitive measure of changes in the available particulate surface area. Such changes are possible by coalescence and sintering, surface contamination, or metal removal from the surface. Since neither Pd evaporation nor diffusion into the bulk mica is likely under the conditions of these experiments, the number of Pd atoms is considered constant.

Coalescence and sintering of supported particles are well-studied effects (*25–30*). We reported earlier that the Pd Auger signal, for a given sample, is reduced after heat treatments, even in the absence of exposure of CO (*3*). This is also accompanied by a small reduction of the CO desorption peak area. However, TEM micrographs of "as-deposited" and heat-treated samples with nominally identical deposits show very little difference and, as mentioned previously, they are representative of nearly all of the metal contributing to CO desorption. Therefore, the reductions of the Pd Auger signal and the CO desorption peak cannot be attributed to large amounts of coalescence. Rather, the reductions appear to be associated with faceting of the particles, possibly by altering the surface-to-volume relationship of the particles.

Contamination derived from CO must involve either carbon atoms, oxygen atoms, or a strongly bound CO molecule. It has been suggested that the CO desorption decay is caused by the loss of Pd particle surface area due to the dispersion into a highly dispersed surface phase of Pd carbonyl (M. Boudart, private communication). Indeed, the binding of CO to a Pd surface is often compared to the CO–Rh bond in the Rh carbonyl, $Rh_6(CO)_{16}$, because of strong spectroscopic similarities (*31*). However, the existence of a Pd carbonyl is still quite doubtful (*32*). This carbonyl hypothesis could not be substantiated experimentally. If it were similar to the Rh carbonyl, which decomposes at about 200°C, it would be expected to decompose during flash thermal desorptions and could not remain as "the contaminant" diminishing the CO peak area as observed. Large-scale dispersion was not observed by TEM when comparing dispersions of strongly "contaminated" Pd deposits and "as-deposited" samples, especially since almost all of the metal could be accounted for by

TEM (Fig. 3b). Appreciable changes in the state of Pd dispersion introduced by FTD of CO or steady-state heating in CO would also be easily detected by changes in the Pd Auger peak height, which was not the case.

Decomposition of CO is not expected to leave oxygen on the Pd surface. Oxygen atoms may leave the Pd surface in a number of ways. First, oxygen may react with CO or H_2, either adsorbed or in background gases, to form CO_2 or H_2O (both reactions are rapid on Pd even at room temperature). Therefore, small quantities of CO_2 or H_2O, produced during CO desorptions, were expected. CO_2 or H_2O production could not be detected during regular CO desorptions or enhanced by an increased background of CO or H_2. Therefore, rapid diffusion of the oxygen into the bulk of the Pd particles or onto the mica surface, depleted of oxygen by cleavage, is assumed most likely.

CO decomposition occurs at a lower temperature on stepped Ni single crystals than on smooth Ni surfaces (*33*). By comparing the results of Castner and Somorjai (*34*) with those of Yates *et al.* (*17*), CO also appears to decompose much more rapidly on stepped rhodium than on smooth Rh (111). In combination with the particle size variation we observed for the CO decomposition rate on both Pd and Ni clusters on mica, CO decomposition appears to be very structure sensitive. The presence of steps, corners, edges, and defects probably has a strong effect on the binding of the CO molecule to some metals. Such edge and corner sites increase rapidly in percentage of the total surface sites with diminishing particle size, especially for the range of particle sizes involved in this work.

The effect of the support also has to be given serious consideration as to differences in chemical behavior between particles and bulk Pd. The tendency of Pd to grow epitaxially on mica is a consequence of a fairly strong metal–support interaction. This could affect the binding of gases to atoms at or near the Pd–mica interface. It may also affect the physical properties of the particles by inducing defects and distortions of the Pd lattice. Future model studies of Pd particles on other oxide support materials with different degrees of metal–support interaction will, therefore, be very informative in assessing the extent of this effect.

SUMMARY AND CONCLUSIONS

CO dissociation on extended Pd surfaces is not expected theoretically (*35*) and has never been observed experimentally on bulk Pd surfaces. Therefore, the observation of CO decomposition on small vapor-grown Pd particles is surprising and controversial. All of the evidence supportive of CO decomposition obtained from this study is summarized:

—The CO desorption peak area decreased with successive thermal desorptions. This decay could not be produced either by heating the Pd/mica sample under UHV or by equivalent exposure to the background gases (at $<5 \times 10^{-10}$ Torr).

—The contaminant preferentially affected the high energy Pd adsorption sites.

—The substantial loss of the CO desorption signal cannot be explained by the simultaneous but comparatively negligible changes in amount and structure of metal observed by the TEM. TEM also accounted for practically all the metal on the mica. Therefore, the coalescence of TEM invisible particles cannot account for large reductions of the desorption peak.

—The ratio of the principal Pd Auger peaks (279 eV/330 eV) increased with the amount of contamination on the surface due to the influence of the carbon 272-eV peak. By subtracting the Auger spectrum of clean Pd on mica from that of a contaminated sample, the small carbon Auger peak can be shown directly.

—Carbon contamination has been produced by heating the sample in a background of CO at a rate similar to that estimated for CO decomposition on Rh (*17*). Carbon can also be produced by electron beam decomposition of CO. Contamination

of both methods affected the CO thermal desorption spectrum in a manner similar to repeated CO adsorption–desorption tests.

—Core electron energy loss spectroscopy of a "contaminated" Pd deposit showed a characteristic carbon peak (without interference from Pd).

—Flash heating a contaminated sample in an oxygen background produced CO_2 from the recombination of carbon and oxygen. (No CO_2 was observed from a clean sample, however.)

—Carbon contamination strongly blocked the CO oxidation reaction.

—The CO thermal desorption results of this study are similar to those found for Ni particles on mica, as reported in the preceding paper (*4*). In the case of Ni, carbon was easily observed by AES, and associative desorption of CO could be produced by dosing a contaminated sample in oxygen.

Some general conclusions important to small-particle surface studies can be drawn from the model catalytic investigations with Pd particles vapor deposited on mica:

—The adsorption stoichiometry of CO on Pd particles appears to be constant up to a size of at least 10 nm. Thus, the CO desorption peak area is a measure of the relative number of available adsorption sites. In combination with the results of AES and TEM measurements, this shows that the growth of Pd on mica is predominantly three dimensional (not singly dispersed) and that almost all of the Pd is detected by standard TEM even for deposits of rather small particles.

—The CO dissociation rate increases rapidly with diminishing particle size, especially for particles smaller than 4 nm in diameter.

—Core electron energy loss spectroscopy can be very useful for detecting C on Pd since the core levels of the two elements are well separated in energy. This is especially valuable since the Auger peaks of C and Pd overlap. However, the small size of the loss signals imposes signal-to-noise limitations.

—Little change in the particle morphology, as seen by TEM, occurs during gas–thermal treatments. Therefore, Pd particles on mica must be considered very stable, especially when compared to Ni (*4*), which underwent drastic changes when subjected to relatively minor gas–thermal treatments.

Future UHV experiments with similar metal–support systems should be of interest, especially for assessing (1) the possible structure sensitivity of other metals for CO decomposition, and (2) the general usefulness of model studies of this nature for understanding practical catalytic processes.

ACKNOWLEDGMENTS

Funds supporting this study were allocated by the Ames Research Center, NASA, Moffett Field, Calif., under Interchange Nos. NCA2-OR840-801 and NCA2-OR840-002. The authors also thank Dr. Lucy Garmon and Professors Martin Prutton and Michel Boudart for helpful discussions, and Dr. Rainer Anton for access to unpublished results of his experiment on the effect of air exposure on small Pd particles.

REFERENCES

1. Thomas, M., Dickinson, J. T., Poppa, H., and Pound, G. M., *J. Vac. Sci. Technol.* **15,** 568 (1978).
2. Thomas, M., Poppa, H., and Pound, G. M., *Thin Solid Films* **58,** 273 (1979).
3. Doering, D. L., Poppa, H., and Dickinson, J. T., *J. Vac. Sci. Technol.* **17,** 198 (1980).
4. Doering, D. L., Dickinson, J. T., and Poppa, H., *J. Catal.* **73,** 91 (1982).
5. Ertl, G., and Koch, J., *in* "Adsorption-Desorption Phenomena" (F. Ricca, Ed.), p. 345. Academic Press, New York, 1972.
6. Conrad, H., Ertl, G., Koch, J., and Latta, E. E., *Surf. Sci.* **43,** 462 (1974).
7. Weissman, D. L., Shek, M. L., and Spicer, W. E., *Surf. Sci.* **92,** L59 (1980).
8. Conrad, H., Ertl, G., and Kuppers, J., *Surf. Sci.* **76,** 323 (1978).
9. Poppa, H., and Elliot, A. G., *Surf. Sci.* **24,** 149 (1971).
10. Tracy, J. C., and Palmberg, P. W., *J. Chem. Phys.* **51,** 4852 (1969).
11. Allpress, J. G., and Sanders, J. V., *Surf. Sci.* **7,** 1 (1967).
12. Redhead, P. A., *Vacuum* **12,** 203 (1962).
13. Brundle, C. R., *J. Vac. Sci. Technol.* **11,** 212 (1974).
14. Anton, R., Ph.D. thesis, Univ. of Hamburg, 1974.

15. Collins, D. M., and Spicer, W. E., *Surf. Sci.* **69,** 85 (19780).
16. Ladas, S., Poppa, H., and Boudart, M., *Surf. Sci.* **102,** 151 (1981).
17. Yates, J. T., Jr., Williams, E. D., and Weinberg, W. H., *Surf. Sci.* **91,** 562 (1980).
18. Muilenberg, G. E. (Ed.), "Handbook of X-Ray Photoelectron Spectroscopy." Perkin–Elmer Corporation, Minn., 1979.
19. McCarty, J. G., and Wise, H., *J. Catal.* **57,** 406 (1979).
20. Engle, T., and Ertl, G., *J. Chem. Phys.* **69,** 1267 (1978).
21. Conrad, H., Ertl, G., Kuppers, J., and Latta, E. E., *Surf. Sci.* **65,** 245 (1977).
22. Ertl, G., and Koch, J., *in* "Proceedings, 5th International Congress on Catalysis, Palm Beach, 1972" (J. W. Hightower, Ed.), p. 67. North-Holland/Elsevier, New York, 1973.
23. Lee, E. H., Ph.D. thesis, Stanford University, 1974.
24. Anderson, J. R., "Structure of Metallic Catalysts," p. 295. Academic Press, New York, 1975.
25. Lewis, B., and Anderson, J. C., "Nucleation and Growth of Thin Films," p. 187. Academic Press, New York, 1978.
26. Poppa, H., and Heinemann, K., *Optik* **56,** 186 (1980).
27. Metois, J. J., Heinemann, K., and Poppa, H., *Appl. Phys. Lett.* **24,** 134 (1976).
28. Ruckenstein, E., and Dadyburjor, D. B., *Thin Solid Films* **55,** 89 (1978).
29. Chen, M., and Schmidt, L. D., *J. Catal.* **56,** 198 (1978).
30. Wynblatt, P., and Ahn, T.-M., *in* "Sintering and Catalysis" (G. C. Kuczynski, Ed.). Plenum, New York, 1975.
31. Ertl, G., *J. Vac. Sci. Technol.* **14,** 435 (1977).
32. Plummer, E. W., Salaneck, W. R., and Miller, J. S., *Phys. Rev. B* **18,** 1673 (1978).
33. Erley, W., and Wagner, H., *Surf. Sci.* **74,** 333 (1978).
34. Castner, D. G., and Somorjai, G. A., *Surf. Sci.* **83,** 60 (1979).
35. Broden, G., Rhodin, T. N., Brucker, C. F., Benbow, R., and Hurych, Z., *Surf. Sci.* **59,** 593 (1976).